Robust state preparation in quantum simulations of Dirac dynamics

Xue-Ke Song,[1,2] Fu-Guo Deng,[2] Lucas Lamata,[1] and J. G. Muga[1]
[1]*Department of Physical Chemistry, University of the Basque Country UPV/EHU, Apartado 644, 48080 Bilbao, Spain*
[2]*Department of Physics, Applied Optics Beijing Area Major Laboratory, Beijing Normal University, Beijing 100875, China*
(Received 12 December 2016; published 22 February 2017)

A nonrelativistic system such as an ultracold trapped ion may perform a quantum simulation of a Dirac equation dynamics under specific conditions. The resulting Hamiltonian and dynamics are highly controllable, but the coupling between momentum and internal levels poses some difficulties to manipulate the internal states accurately in wave packets. We use invariants of motion to inverse engineer robust population inversion processes with a homogeneous, time-dependent simulated electric field. This exemplifies the usefulness of inverse-engineering techniques to improve the performance of quantum simulation protocols.

DOI: 10.1103/PhysRevA.95.022332

I. INTRODUCTION

A recent highlight in the remarkable history of the Dirac equation [1,2] is the realization that nonrelativistic systems such as an ultracold trapped ion can obey this equation, with a proper reinterpretation of symbols, under specific trapping conditions and laser interactions [3–6]. In a one-dimensional setting (linear trap), two levels of the ion interacting with laser fields set the basis that spans the relevant internal state subspace, whereas orthogonal eigenvectors of the Dirac Hamiltonian with positive and negative energies correspond to matter and antimatter solutions. Similarly, different elements of the original Dirac equation, such as the mass, or the constant playing the role of speed of light, are mapped to atomic or interaction-dependent properties. Different interaction potentials may also be simulated, such as the ones for homogeneous or linear electric fields [5]. These mappings and the controllability of trapped ions have been used to observe experimentally simulations of relativistic effects, like Zitterbewegung [4], or Klein tunneling [6]. Trapped ions are in fact an example of a wider set of nonrelativistic "Dirac systems" that obey a Dirac dynamics, for example in condensed matter [7], optics [8], cold atoms [9,10], or superconducting circuits [11].

The new physical platforms for Dirac dynamics are often easier to manipulate than relativistic particles. In trapped ions, for example, the effective (simulated) mass, speed of light, or electric field may be changed in time. This opens prospects for finding and implementing new or exotic effects and carrying out further fundamental studies. It also motivates a search for manipulation protocols to achieve specific goals [12]. Shortcuts to adiabaticity (STAs) [13], a group of techniques to speed up adiabatic methods, possibly following nonadiabatic routes, offer a suitable framework for the task, and example cases have been worked out recently in the domain of the Dirac equation [12,14]. STAs are typically highly flexible so that, apart from speeding up the processes, which may be needed to avoid decoherence, the protocol may satisfy further conditions, such as robustness with respect to noise and/or systematic perturbations. Robust protocols have been demonstrated for the Schrödinger equation [15,16], and, as we shall see in this paper, can be extended as well to the Dirac equation.

The study case we address here is a population inversion of the internal state, as a paradigmatic example of single qubit operations, making use of an effective time-dependent, homogeneous electric field. Due to the structure of the Dirac Hamiltonian, a protocol designed to perform the inversion for a specific momentum, say the average momentum of the wave packet, in general will not work perfectly for other momenta. In other words, the momentum spread is a source of systematic errors, and our goal will be to design robust protocols with respect to momentum offsets inherent in wave packets. The employment of inverse engineering and STA methods may enhance the toolbox of quantum simulations and enable faster and more accurate protocols, which will presumably boost the field of quantum technologies.

The paper is organized as follows: In Sec. II we set the model and Hamiltonian. In Sec. III we give the solution via invariants. In Sec. IV, we put forward a robust invariant-based protocol to engineer the quantum state. Section V analyzes the robustness of the invariant-based shortcut protocols against the systematic momentum error. Section VI addresses a proposal to implement the robust protocol via a Dirac equation dynamics using trapped ions. Finally Sec. VII summarizes and discusses the results.

II. DRIVEN DIRAC DYNAMICS WITH TIME-DEPENDENT VECTOR FIELD

We focus now on a $1+1$-dimensional Dirac equation for a charged particle moving in x direction, which could be simulated by ultracold trapped ions and realizes quantum relativistic effects [3–5]. It may be written as [12]

$$i\hbar|\dot{\Psi}(t)\rangle = \{[-i\hbar c\partial_x + A(x,t)]\sigma_x + mc^2\sigma_z\}|\Psi(t)\rangle, \quad (1)$$

where $|\Psi(t)\rangle$ is the two-component time-dependent wave function for the particle with mass m, the dot means time derivative, c is the speed of light, which should be considered as a constant in the simulation, $\hbar$ is the Planck constant divided by 2π, and $\sigma_{x,y,z}$ are 2×2 Pauli matrices in the basis

$$|1\rangle = \begin{pmatrix}1\\0\end{pmatrix}$$

and

$$|2\rangle = \begin{pmatrix}0\\1\end{pmatrix}.$$

 ©2017 American Physical Society

To implement a time-dependent but spatially homogeneous electric field, we set $A(x,t)$ as a purely time-dependent function, $A(x,t) = \alpha_t$. Then the Hamiltonian reads

$$H = -i\hbar c\partial_x\sigma_x + \alpha_t\sigma_x + mc^2\sigma_z. \tag{2}$$

Beware that c, m, and the electric field must be reinterpreted in the simulated dynamics, as discussed in [3–5] and later in Sec. VI. Note also that, whereas the two components of the state do not represent the spin in the relativistic interpretation [17], the two levels $|1\rangle$ and $|2\rangle$ in the simulation simply become two bare internal levels of the ion.

Deffner [12] used the fast-forward shortcut technique [18,19] to suppress "production of pairs" (transitions among positive and negative energy solutions) in fast processes, combining scalar and pseudoscalar potentials. Our goal here is instead to induce a fast and robust population inversion among the bare levels. A different technique will be applied, designing the time dependence of the parameters in the Hamiltonian rather than adding terms to it. This is carried out by making use of invariants of motion twice: first to decompose the solution of the Dirac equation into independent subspaces for each plane wave, and then to describe and manipulate the solution for the internal state amplitudes within each subspace [14].

III. SOLUTIONS VIA INVARIANTS

We shall find exact solutions of the Dirac equation in Eq. (1) based on the Lewis and Riesenfeld theory of invariants [20]. For the Hamiltonian in Eq. (2), let us assume that a nontrivial invariant exists with the form [21–23]

$$I = A(t)p + B(t)x + D(t), \tag{3}$$

where $A(t)$, $B(t)$, and $D(t)$ are 2×2 matrices. The invariant should satisfy the equation

$$\frac{dI}{dt} = \frac{1}{i\hbar}[I,H] + \frac{\partial I}{\partial t} = 0. \tag{4}$$

Substituting Eqs. (2) and (3) into Eq. (4) gives

$$[A,\sigma_x] = 0, \tag{5}$$

$$[B,\sigma_x] = 0, \tag{6}$$

$$\alpha_t[A,\sigma_x] + mc^2[A,\sigma_z] + c[D,\sigma_x] + i\hbar\dot{A} = 0, \tag{7}$$

$$\alpha_t[B,\sigma_x] + mc^2[B,\sigma_z] + i\hbar\dot{B} = 0, \tag{8}$$

$$i\hbar cB\sigma_x + \alpha_t[D,\sigma_x] + mc^2[D,\sigma_z] + i\hbar\dot{D} = 0. \tag{9}$$

Expanding the matrices in the su(2) basis, $A = a_1 + a_2\sigma_x + a_3\sigma_y + a_4\sigma_z$ with a_i an arbitrary real number for $i = 1,2,3,4$, and similarly for B and D, the above equations are easy to solve. From Eqs. (5) and (6), we get

$$A = a_1 + a_2\sigma_x, \tag{10}$$

$$B = b_1 + b_2\sigma_x, \tag{11}$$

where a_1, a_2, b_1, b_2 are to be determined. Substituting Eq. (11) into Eq. (8), we have

$$\dot{b}_1 = \dot{b}_2 = 0, \tag{12}$$

$$b_2 = 0. \tag{13}$$

Substituting Eq. (10) into Eq. (7), we have

$$\begin{aligned} cd_4 &= mc^2a_2, \\ d_3 &= 0, \\ \dot{a}_1 &= \dot{a}_2 = 0. \end{aligned} \tag{14}$$

Similarly, from Eq. (9), we find

$$\begin{aligned} cb_1 + \dot{d}_2 &= 0, \\ \alpha_t d_4 &= mc^2 d_2, \\ \dot{d}_1 &= \dot{d}_4 = 0. \end{aligned} \tag{15}$$

The invariant can be then written as

$$I = (a_1p + b_1x + d_1) + (a_2p + d_2)\sigma_x + d_4\sigma_z, \tag{16}$$

where a_1, a_2, b_1, d_1, and d_4 are constant. If α_t is time dependent, then $d_4 = d_2 = 0$, and therefore $b_1 = a_2 = 0$. The invariant can be simplified as

$$I = a_1p + d_1 = a_1(p + \mathbb{C}), \tag{17}$$

where $\mathbb{C}$ is a constant. This holds even for a time-dependent mass. Consistently, the Heisenberg equations of motion for the Hamiltonian (2) are

$$\frac{dp}{dt} = 0, \quad \frac{dx}{dt} = c\sigma_x. \tag{18}$$

In other words, the momentum operator is invariant, which may be interpreted as the initial momentum p_0 [24], as shown below making use of a different frame.

The solutions of the time-dependent Dirac equation may be written as linear superpositions of eigenvectors of the invariant [20]. Since the eigenfunctions of the invariant take the plane-wave form $e^{ip_0x/\hbar}$ with p_0 a real number, we assume the existence of plane-wave solutions of Eq. (1) according to the *Ansatz*

$$|\phi(t)\rangle = e^{ip_0x/\hbar}|\phi_{p_0}(t)\rangle, \tag{19}$$

where $|\phi_{p_0}(t)\rangle$ is a 2×1 vector that depends on the parameters p_0 and t.

Substituting Eq. (19) into the time-dependent Dirac equation (1) gives the following reduced (2×2) Dirac equation for the vector $|\phi_{p_0}(t)\rangle$:

$$i\hbar|\dot{\phi}_{p_0}(t)\rangle = H_{p_0}|\phi_{p_0}(t)\rangle, \tag{20}$$

where

$$H_{p_0} = cp_0\sigma_x + \alpha_t\sigma_x + mc^2\sigma_z. \tag{21}$$

By superposing plane-wave solutions, general (wave packet) solutions are found, of the form

$$|\Psi(t)\rangle = \int_{-\infty}^{\infty} a(p_0)|\phi_{p_0}(t)\rangle dp_0, \tag{22}$$

where each (momentum) component evolves with its own 2×2 Hamiltonian H_{p_0}, so that the corresponding global (wave packet) populations for $|1\rangle$ and $|2\rangle$ are given by

$$P_k = \int_{-\infty}^{\infty} |a(p_0)|^2 P_k(p_0) dp_0, \tag{23}$$

where $k = 1,2$ and $P_k(p_0) = |\langle k|\phi_{p_0}(t)\rangle|^2$ $(k = 1,2)$ are the populations for each momentum in the basis $\{|1\rangle,|2\rangle\}$. In the numerical examples we take a Gaussian function $|a(p_0)|^2 = \frac{1}{\sqrt{2\pi}\sigma} \exp(-p_0^2/\sigma^2)$.

The homogeneous electric field is more often represented by a linear scalar potential. To find this representation and see the equivalence with our treatment, we change the frame by means of the unitary transformation $U = e^{-i\alpha_t x/(\hbar c)}$. The effective Hamiltonian becomes

$$H_u = U^\dagger H U - i\hbar U^\dagger \dot{U} = cp\sigma_x + mc^2\sigma_z - \dot{\alpha}_t x/c, \tag{24}$$

where we have used the Hausdorff expansion, which can be truncated here exactly, as $e^{\xi x} H e^{-\xi x} = H + \xi[x,H]$, with $\xi = i\alpha_t/(\hbar c)$. The homogeneous field is now represented by a linear scalar potential of time-varying slope. The plane-wave solutions transform as $|\phi_u(t)\rangle = U^\dagger|\phi(t)\rangle = e^{i(p_0+\alpha_t/c)x/\hbar}|\phi_{p_0}(t)\rangle$ so they get a time-dependent momentum and the invariant of H_u becomes [as it may be seen by repeating the steps after Eq. (4) for H_u] $I_u = \mathbb{C}(p - \alpha_t/c)$. Since the two frames are unitarily connected, in what follows we shall use for simplicity the one based on H.

IV. ROBUST QUANTUM STATE ENGINEERING

A. Invariant-based shortcuts to adiabaticity for driven Dirac dynamics

The Hamiltonian H_{p_0} in (21) for the Dirac system with spatially homogeneous electric field reads in matrix form

$$H_{p_0} = \begin{pmatrix} mc^2 & cp_0 + \alpha_t \\ cp_0 + \alpha_t & -mc^2 \end{pmatrix}. \tag{25}$$

If the functions of time $m(t)$ and α_t are given, different values of p_0 imply different 2×2 Hamiltonians, with different solutions of the Dirac equation (20). If we design $m(t)$ and α_t by inverse engineering so as to induce a population inversion (or some other operation), say at $p_0 = 0$, which we assume to be the average momentum of a wave packet, the solution for any other momentum will generally fail to satisfy the intended task. In other words, the spread of p_0 in a wave packet can affect the dynamics and induce errors. Therefore, it is necessary to design protocols robust with respect to the momentum spread. The perturbed Hamiltonian H_{p_0} can be decomposed as $H_{p_0} = H_0(t) + H_1(t)$, where

$$H_0(t) = \begin{pmatrix} mc^2 & \alpha_t \\ \alpha_t & -mc^2 \end{pmatrix}$$

is the unperturbed Hamiltonian and

$$H_1(t) = c\begin{pmatrix} 0 & p_0 \\ p_0 & 0 \end{pmatrix}$$

is the "systematic error" Hamiltonian. In the following, adopting the standard notation for two-level Hamiltonians in quantum optics, $\frac{\hbar}{2}\Delta(t) = mc^2$ and $\frac{\hbar}{2}\Omega(t) = \alpha_t$, in terms of a detuning Δ, and a Rabi frequency Ω, we write

$$H_0(t) = \frac{\hbar}{2}\begin{pmatrix} \Delta & \Omega \\ \Omega & -\Delta \end{pmatrix}. \tag{26}$$

The instantaneous adiabatic eigenstates of $H_0(t)$ are

$$|E_+(t)\rangle = \cos\left(\frac{\varphi}{2}\right)|1\rangle + \sin\left(\frac{\varphi}{2}\right)|2\rangle, \tag{27}$$

$$|E_-(t)\rangle = \sin\left(\frac{\varphi}{2}\right)|1\rangle - \cos\left(\frac{\varphi}{2}\right)|2\rangle, \tag{28}$$

with the mixing angle $\varphi = \arctan(\Omega/\Delta)$ and the corresponding adiabatic energies $E_\pm(t) = \pm\frac{\hbar}{2}\sqrt{\Delta^2+\Omega^2}$.

For this time-dependent 2×2 Hamiltonian H_0, there exists a dynamical invariant I_0, not to be confused with the momentum invariant of Eq. (2). This invariant in the internal-state subspace can be written as [13,20,25,26]

$$I_0(t) = \frac{\hbar}{2}\Omega_0\begin{pmatrix} \cos\theta & \sin\theta e^{i\beta} \\ \sin\theta e^{-i\beta} & -\cos\theta \end{pmatrix}, \tag{29}$$

where Ω_0 is an arbitrary constant (angular) frequency to keep $I_0(t)$ with dimensions of energy, and θ and β are auxiliary time-dependent angles. Using Eqs. (26) and (29) in Eq. (4) we find the differential equations

$$\dot{\theta} = \Omega\sin\beta, \tag{30}$$

$$\dot{\beta} = \Omega\cot\theta\cos\beta - \Delta. \tag{31}$$

The eigenstates of the invariant are

$$|\phi_+(t)\rangle = \begin{pmatrix} \cos(\theta/2)e^{i\beta/2} \\ \sin(\theta/2)e^{-i\beta/2} \end{pmatrix}, \tag{32}$$

$$|\phi_-(t)\rangle = \begin{pmatrix} \sin(\theta/2)e^{i\beta/2} \\ -\cos(\theta/2)e^{-i\beta/2} \end{pmatrix}, \tag{33}$$

which satisfy $I_0|\phi_n(t)\rangle = \lambda_n|\phi_n(t)\rangle (n = \pm)$ with the eigenvalues $\lambda_\pm = \pm\hbar\Omega_0/2$. The general solution of the time-dependent Schrödinger equation, according to the theory of Lewis and Riesenfeld [20], can be written as a linear combination $|\Phi_s\rangle = \sum_{n=\pm} c_n e^{i\epsilon_n}|\phi_n\rangle$, where $c_\pm$ are time-independent amplitudes, and the $\epsilon_\pm$ are the Lewis-Riesenfeld phases,

$$\epsilon_\pm(t) = \frac{1}{\hbar}\int_0^t \langle\phi_\pm(t')|i\hbar\frac{\partial}{\partial t'} - H_0(t')|\phi_\pm(t')\rangle dt'. \tag{34}$$

Then, two orthogonal solutions can be constructed as

$$|\psi_0(t)\rangle = e^{-i\gamma(t)/2}|\phi_+(t)\rangle = e^{-i\gamma(t)/2}\begin{pmatrix} \cos(\theta/2)e^{i\beta/2} \\ \sin(\theta/2)e^{-i\beta/2} \end{pmatrix}, \tag{35}$$

and

$$|\psi_\perp(t)\rangle = e^{i\gamma(t)/2}|\phi_-(t)\rangle = e^{i\gamma(t)/2}\begin{pmatrix} \sin(\theta/2)e^{i\beta/2} \\ -\cos(\theta/2)e^{-i\beta/2} \end{pmatrix}, \tag{36}$$

where $\gamma = 2\epsilon_- = -2\epsilon_+$ and $\langle\psi_0(t)|\psi_\perp(t)\rangle = 0$ for all times. Thus, by using Eqs. (30) and (34), we find

$$\dot{\gamma} = \frac{\Omega\cos\beta}{\sin\theta} = \frac{\dot{\theta}\cos\beta}{\sin\theta\sin\beta}. \tag{37}$$

Our aim is to design invariant-based shortcuts to achieve a population inversion from state $|1\rangle$ to state $|2\rangle$, up to a global phase factor, along the invariant eigenstate $|\phi_+(t)\rangle$ in a given time t_f. We therefore write down the boundary conditions for θ to guarantee the desired initial and final states,

$$\theta(0) = 0, \quad \theta(t_f) = \pi. \tag{38}$$

Moreover, if we impose $[H_0(0), I_0(0)] = 0$ and $[H_0(t_f), I_0(t_f)] = 0$ so that the Hamiltonian $H_0(t)$ and the invariant $I_0(t)$ share common eigenstates at initial and final times, we have the additional boundary conditions

$$\Omega(0) = 0, \quad \dot{\theta}(0) = 0,$$
$$\Omega(t_f) = 0, \quad \dot{\theta}(t_f) = 0. \tag{39}$$

The Rabi frequency and detuning leading to a fast population inversion are determined from Eqs. (30) and (31), choosing a convenient function of β, and interpolating θ to satisfy the boundary conditions (38) and (39).

B. Robust shortcuts against systematic momentum errors

To construct invariant-based shortcuts robust against the systematic momentum errors, we use perturbation theory up to $\mathcal{O}(p_0^2)$ to find the time evolution of the quantum state governed by H_{p_0} that starts as $|\psi_0(0)\rangle$,

$$|\psi(t_f)\rangle = |\psi_0(t_f)\rangle - \frac{i}{\hbar}\int_0^{t_f} dt \hat{U}_0(t_f,t)H_1(t)|\psi_0(t)\rangle$$
$$- \frac{1}{\hbar^2}\int_0^{t_f} dt \int_0^{t} dt' \hat{U}_0(t_f,t)H_1(t)$$
$$\times \hat{U}_0(t,t')H_1(t')|\psi_0(t')\rangle + \cdots, \tag{40}$$

where $|\psi_0(t)\rangle$ is the unperturbed solution and $\hat{U}_0(s,t) = |\psi_0(s)\rangle\langle\psi_0(t)| + |\psi_\perp(s)\rangle\langle\psi_\perp(t)|$ is the unperturbed time evolution operator. We assume that the error-free ($p_0 = 0$) scheme works perfectly, i.e., $|\psi_0(0)\rangle = |1\rangle$, $|\psi_0(t_f)\rangle = |2\rangle$, up to phase factors. Then, the probability of the excited state at the final time for t_f and momentum p_0 is

$$P_2(p_0) = |\langle\psi_0(t_f)|\psi(t_f)\rangle|^2$$
$$= 1 - \frac{1}{\hbar^2}\left|\int_0^{t_f} dt \langle\psi_\perp(t)|H_1(t)|\psi_0(t)\rangle\right|^2. \tag{41}$$

Defining the systematic error sensitivity as [15,16]

$$q_s := -\frac{1}{2}\frac{\partial^2 P_2(p_0)}{\partial p_0^2}\bigg|_{p_0=0} = -\frac{\partial P_2(p_0)}{\partial (p_0^2)}\bigg|_{p_0=0}, \tag{42}$$

we have

$$q_s = \frac{c^2}{\hbar^2}\left|\int_0^{t_f} dt e^{-i\gamma}(-i\sin\beta - \cos\theta\cos\beta)\right|^2. \tag{43}$$

For a flat π pulse, $\beta = \pi/2$, and $\theta = \pi t/t_f$, so $\dot{\theta} = \pi/t_f$, $\Omega = \pi/t_f$, $\Delta = 0$, and $\dot{\gamma} = 0$. This gives

$$q_s(\pi \text{ pulse}) = \frac{c^2 t_f^2}{\hbar^2}. \tag{44}$$

Optimally robust invariant-based shortcuts are now defined as those that make the systematic error sensitivity zero. Following [27], we could try the simple Fourier series type of *Ansatz*

$$\gamma = 2\theta + \nu\sin(2\theta), \tag{45}$$

where ν is a real number that may be varied to nullify q_s. (It is possible to extended this *Ansatz* to make further derivatives zero as in [27].) Alternatively we use [15]

$$\gamma = \nu[2\theta - \sin(2\theta)]. \tag{46}$$

Both *Ansätze* are valid and nullify q_s for different values of ν. They lead approximately to the same pulse area $A = \int_0^{t_f}\Omega(t)dt$, but the second one provides simpler expressions of β, Ω, and Δ, using Eqs. (30), (31), and (37), so it is preferred here. Specifically, using Eqs. (37) and (46), the parameter β takes the form

$$\beta = \text{arccot}(4\nu\sin^3\theta). \tag{47}$$

This gives $\beta(0) = \beta(t_f) = \pi/2$ so that the invariant eigenstate $|\phi_+(t)\rangle$, see Eq. (32), evolves from $|1\rangle$ to $|2\rangle$ up to phase factors, $|\phi_+(0)\rangle = e^{i\pi/4}|1\rangle$ and $|\phi_+(t_f)\rangle = e^{-i\pi/4}|2\rangle$. Finally, the systematic errors sensitivity is given by

$$q_s = \frac{c^2}{\hbar^2}\left|\int_0^{t_f} dt e^{-i\nu[2\theta-\sin(2\theta)]}\frac{-i - 4\nu\sin^3\theta\cos\theta}{\sqrt{1+16\nu^2\sin^6\theta}}\right|^2. \tag{48}$$

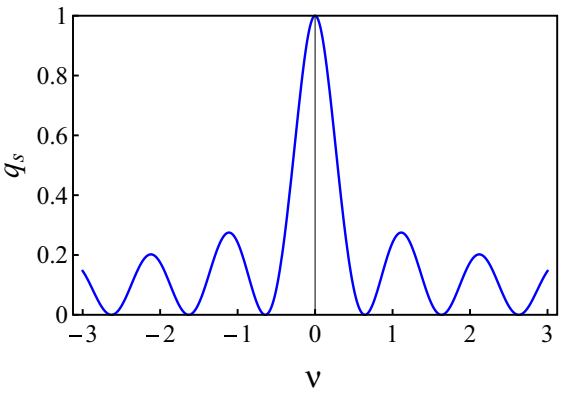

FIG. 1. Systematic error sensitivity q_s in Eq. (48). As in all figures we use dimensionless units with $c = \hbar = t_f = 1$. For specific values of $|\nu|$, $q_s = 0$ is satisfied, in particular at the minimal value $|\nu| = 0.643$.

Figure 1 shows the systematic error sensitivity versus ν, passing through zeroes of q_s. (In all numerical calculations we use dimensionless units with $c = \hbar = t_f = 1$. The dimensionless effective mass generally depends on time so it is not made 1 as usual.) The corresponding Rabi frequency and detuning are

$$\Omega = \dot{\theta}\sqrt{1+16\nu^2\sin^6\theta}, \tag{49}$$

$$\Delta = 16\nu\sin^2\theta\cos\theta\,\dot{\theta}\frac{1+4\nu^2\sin^6\theta}{1+16\nu^2\sin^6\theta}. \tag{50}$$

Ω increases monotonously with ν so we choose the smaller value consistent with $q_s = 0$, $\nu_m = 0.643$, to minimize Ω along the evolution path. In addition, to interpolate at intermediate times, we assume a polynomial *Ansatz* $\theta = \sum_{j=0}^{3} a_j t^j$, where the coefficients a_j are found by solving the equations set by the boundary conditions on θ and its derivative; see Eqs. (38)

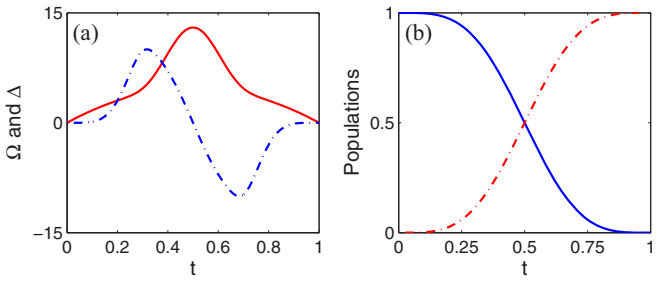

FIG. 2. (a) The Rabi frequency Ω (red, solid line) and detuning Δ (blue, dotted-dashed line) in our optimal protocol. (b) Time evolution of the populations $P_1(0)$ (blue, solid line) and $P_2(0)$ (red, dotted-dashed line) during the population inversion. We have used $\nu = 0.643$ and $p_0 = 0$.

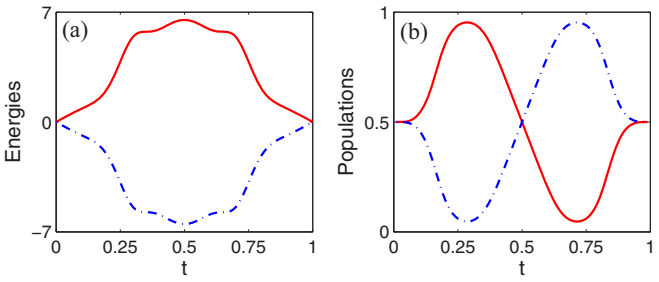

FIG. 4. (a) The adiabatic energies of Hamiltonian $H_0(t)$: $E_+(t)$ (red, solid line) and $E_-(t)$ (blue, dotted-dashed line). (b) The adiabatic time evolution of the populations of level $|1\rangle$ for the positive (red, solid line) and negative (blue, dotted-dashed line) energy eigenstates of Hamiltonian $H_0(t)$. Ω and Δ are as in Fig. 2(a).

and (39). The time-dependent Ω and Δ are shown in Fig. 2(a), with absolute value maxima $|\Omega_m| \simeq 13$ and $|\Delta_m| \simeq 10$. For the specified $H_0(t)$ in Eq. (26), corresponding to $p_0 = 0$, we solve $H_0|\phi_0(t)\rangle = i\hbar|\dot{\phi}_0(t)\rangle$ numerically by a Runge-Kutta method with an adaptive step, and get the time evolution of the populations $P_k(p_0 = 0)$ for the optimal protocol represented in Fig. 2(a). Figure 2(b) shows the population inversion between $|1\rangle$ and $|2\rangle$. By contrast, solving the dynamics separately for each p_0 with H_{p_0}, and averaging the populations $P_k(p_0)$ according to Eq. (23), Fig. 3 shows the change of the global population P_k for Gaussian wave packets with $\sigma = 0.3$ and $\sigma = 0.9$, respectively. The population inversion is still accurate for $\sigma = 0.3$, but by further increasing the momentum width, it eventually must fail. $P_2(p_0)$ is shown in the next section, making explicit the momentum-width window where a perfect inversion can be achieved.

We plot the adiabatic (instantaneous) eigenenergies of $H_0(t)$ in Fig. 4(a) for the optimal protocol. Note the degeneracy at the edge times due to the vanishing of Δ and Ω. Figure 4(b) depicts the adiabatic time evolution of the populations of level $|1\rangle$ in both eigenstates, $|\langle 1|E_+(t)\rangle|^2$ and $|\langle 1|E_-(t)\rangle|^2$. In addition, Fig. 5 depicts the instantaneous populations of positive and negative energy eigenstates for the invariant eigenstates, $|\langle E_+(t)|\phi_+(t)\rangle|^2$ and $|\langle E_-(t)|\phi_+(t)\rangle|^2$. While the positive energy solution dominates most of the time, both are equally important at boundary times.

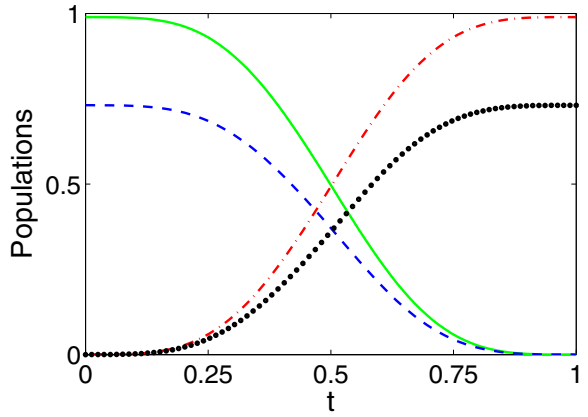

FIG. 3. Time evolution of the populations P_1 of a Gaussian wave packet centered at zero momentum (green, solid line and blue, dot-dashed line for $\sigma = 0.3$ and $\sigma = 0.9$, respectively) and P_2 (red, dotted-dashed line and black circles for $\sigma = 0.3$ and $\sigma = 0.9$, respectively) by averaging over all momenta p_0, see Eq. (23), during the population inversion. H_0 as in Fig. 2(a). Compare to the result for a plane wave, $p_0 = 0$, in Fig. 2(b).

V. ROBUSTNESS AGAINST WAVE-PACKET MOMENTUM SPREAD

We now test the stability of the optimal invariant-based protocol of the previous section with respect to the momentum spread in wave packets, compared to a simple invariant-based shortcut for which the sensitivity is not zero. Both protocols should invert the population along the invariant eigenstate $|\phi_+(t)\rangle$ in a given time t_f for $p_0 = 0$. Let us denote by a subscript "s" the auxiliary angles $\theta_s(t)$ and $\beta_s(t)$ and the Hamiltonian functions Ω_s, Δ_s for the simple protocol with nonzero sensitivity. To perform a fair comparison, we impose the same maxima of Rabi frequency and detuning for the two protocols. We also take $\theta_s(t) = \theta(t)$ and $\beta_s(0) = \beta_s(t_f) = \pi/2$ for simplicity. Setting $\beta_s(t_f/2) = 2\pi/17$ the maximum of the Rabi frequency becomes $\Omega_s^m \simeq 13$, as in the optimal

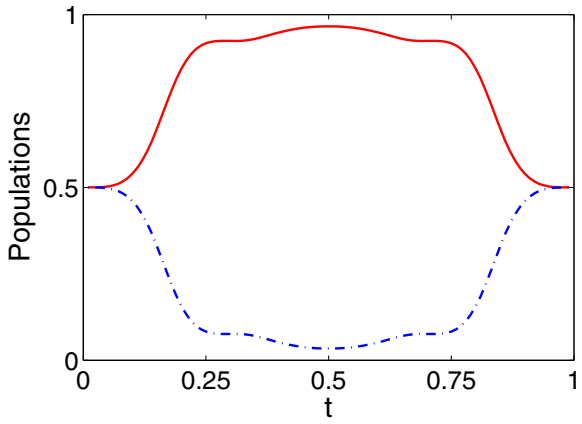

FIG. 5. Populations of energy eigenstates along the invariant eigenstate $|\phi_+(t)\rangle$, $|\langle E_+(t)|\phi_+(t)\rangle|^2$ (red, solid line) and $|\langle E_-(t)|\phi_+(t)\rangle|^2$ (blue, dotted-dashed line), for the optimal $\Omega(t)$ and $\Delta(t)$ in Fig. 2(a).

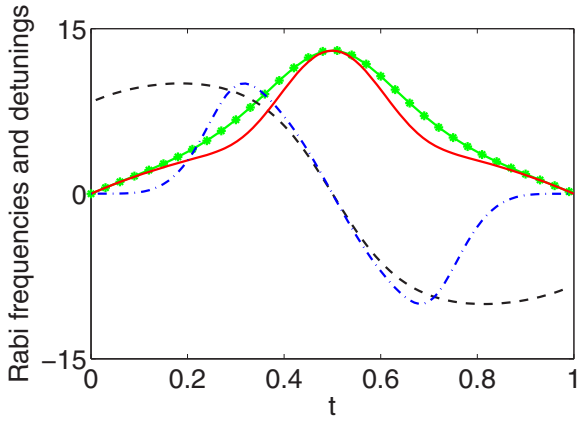

FIG. 6. The Rabi frequency Ω_s (green, dotted-star line), and detuning and Δ_s (black, dashed line) are determined by Eqs. (30) and (31) with angles $\theta_s(t)=\sum_{j=0}^{3}a_j t^j$ and $\beta_s(t)=\sum_{j=0}^{4}b_j t^j$ in simple invariant-based shortcuts, together with "optimal" $\Omega(t)$ (red, solid line) and $\Delta(t)$ (blue, dotted-dashed line) in Fig. 2(a).

invariant-based shortcut. Moreover, the derivative of $\beta_s(t)$ at boundary times is chosen as $\dot{\beta}_s(0)=-\dot{\beta}_s(t_f)=-15\pi/(17t_f)$, so that the maximal detuning $|\Delta_s^m|\simeq 10$ at initial and final times is the same as for the optimal protocol. $\beta_s(t)$ is interpolated at intermediate times with a polynomial *Ansatz* $\beta_s(t)=\sum_{j=0}^{4}b_j t^j$, where the coefficients b_j are found by solving the boundary conditions. With the determined $\beta_s(t)$ and $\theta_s(t)$, the Rabi frequency $\Omega_s(t)$ and detuning $\Delta_s(t)$ in the simple invariant-based shortcut can be calculated from Eqs. (30) and (31). They are plotted in Fig. 6, together with the Rabi frequency and detuning of the optimal protocol of Fig. 2(a), which in fact has a slightly smaller pulse area. By making use of Eq. (25) with $mc^2=\frac{\hbar}{2}\Delta(t)$ and $\alpha_t=\frac{\hbar}{2}\Omega(t)$ to solve numerically Eq. (20) with the initial state $|1\rangle$, the excitation probabilities $P_2(p_0)$ at final time $t_f=1$ based on the different invariant-based shortcuts are depicted in Fig. 7, which demonstrates the robustness of the optimal protocol. If needed, it is possible to systematically increase the width of

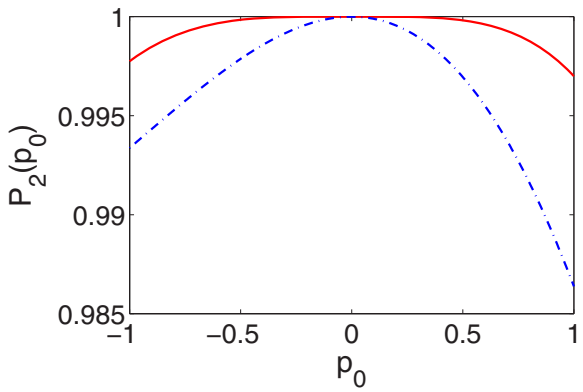

FIG. 7. Probability $P_2(p_0)$ at the final time $t_f=1$ vs systematic momentum noise p_0 by solving numerically Eq. (20) with the Hamiltonian (25) based on the optimal invariant-based shortcut of Fig. 2(a) (zero sensitivity, red, solid line), and simple ones (nonzero sensitivity, blue, dotted-dashed line).

the plateau as in [27], by nullifying higher derivatives of the population at $p_0=0$.

VI. TRAPPED-ION IMPLEMENTATION

Even though the basic structure of a trapped-ion implementation of a $1+1$ Dirac equation was already proposed in Refs. [3–5], in our current formalism the simulated mass and electric field should be time dependent and highly controllable. The high degree of laser control in trapped ions enables this kind of approach, given that laser amplitudes can be turned on and off *in situ* and their profiles designed according to the requirements of the proposed protocol.

In the Lamb-Dicke regime, the Hamiltonian describing the carrier interaction of a pair of internal levels of a single ion with mass M driven by a laser field takes the form of $H_c=\hbar\Omega_c(\sigma^+e^{i\phi_c}+\sigma^-e^{-i\phi_c})$, where $\eta=k\sqrt{\hbar/2M\nu_0}$ is the Lamb-Dicke parameter [28,29] with k the wave number of the driving field and ν_0 the frequency of a center-of-mass mode, Ω_c is the Rabi frequency, ϕ_c is the field phase, and σ^+ (σ^-) is the raising (lowering) ionic spin-1/2 operator. A Jaynes-Cummings (JC) Hamiltonian, also known as red-sideband interaction, $H_r=\hbar\tilde{\Omega}_r\eta(\sigma^+ae^{i\phi_r}+\sigma^-a^\dagger e^{-i\phi_r})$, couples the two internal levels of the ion and one of the vibrational center-of-mass modes, where a ($a^\dagger$) is the annihilation (creation) operators of the vibrational mode. In the blue motional sideband, also known as anti-JC (AJC) interaction, the Hamiltonian can be written as $H_b=\hbar\tilde{\Omega}_b\eta(\sigma^+a^\dagger e^{i\phi_b}+\sigma^-ae^{-i\phi_b})$, where $\tilde{\Omega}_{r(b)}$ and $\phi_{r(b)}$ are the Rabi frequency and phase of the light field. By applying all of these interactions simultaneously with appropriate Rabi frequencies and relative phases, the Dirac Hamiltonian for a free particle, $H_{\rm free}=c\sigma_x p+mc^2\sigma_y$, can be completely mapped by making the identifications $mc^2:=\hbar\Omega_c$, and $c:=2\eta\Lambda\tilde{\Omega}_1$ [3,4]. Here, $p=i\hbar(a^\dagger-a)/2\Lambda$ with $\Lambda=\sqrt{\hbar/4M\nu_0}$ the size of zero-point wave packet, and $\tilde{\Omega}_1=\tilde{\Omega}_r=\tilde{\Omega}_b$. We point out that the carrier can generate a mass term with a σ_y Pauli matrix at lowest order, which contains the same physics as the σ_z, given that the same Clifford algebra is satisfied. Another possibility that does not employ the carrier is via a detuning in the red and blue sideband pulses, which will directly generate the σ_z term in an appropriate interaction picture. In general, a time-dependent Rabi frequency Ω_c or detuning will induce a simulated time-dependent mass in the Dirac system, as our protocol does. In addition, as shown in [5,6], a free Dirac equation can be encoded by a single ion (ion 1), and external potentials can be implemented by a second ion (ion 2) driven by another bichromatic light field with same vibrational mode but a different electronic transition. For example, by imposing a laser field with appropriate phases and a time-dependent Rabi frequency $\tilde{\Omega}_2$ on the ion 2, the Hamiltonian for the two-ion system will take the form of $H_e=c\sigma_x p+mc^2\sigma_z-e\phi_e$, where $-e$ is the electron charge, ϕ_e is a nonzero electric potential, $e\phi_e:=g(t)\sigma_x^{(2)}x$ with $g(t)=\hbar\eta\tilde{\Omega}_2(t)/\Lambda$, and $x=(a+a^\dagger)\Lambda$ is the position operator [5]. If ion 2 is prepared in the positive eigenstate of Pauli operator $\sigma_x^{(2)}$, this operator could be replaced by its $+1$ eigenvalue, and this reduces to a linear potential in the Hamiltonian H_e, which is in consistent with the Hamiltonian H_u in Eq. (24), with $\dot{\alpha}_t/c:=g(t)$. Up to a unitary transformation $U^\dagger=e^{i\alpha_t x/(\hbar c)}$, the Hamiltonian H of Eq. (2) is found. Thus, the optimal

robust quantum state engineering protocol in Dirac dynamics can be effectively mapped by a string of two trapped ions. Alternatively, the synthetic electric field may be implemented directly in H without a second ion with a proper pulse. Unlike the Schrödinger equation, a π-carrier pulse for Dirac dynamics does not invert the population perfectly for a wave packet, see Eq. (44), due to the first term in H, a problem that may be solved by inverse-engineered optimized pulses as the ones proposed in Sec. IV.

VII. DISCUSSION AND SUMMARY

Different systems that behave according to the same model equations—with disparate interpretation of the symbols—simulate each other. Often one of these systems is easier to control and manipulate. It may also obey the model for a domain of parameters hard or impossible to implement in the other one leading to exotic phenomena. Dirac systems obeying the Dirac equation represent well this scenario and offer manipulation possibilities much beyond the ones for the domain of spin-1/2 relativistic particles. In line with the current interest to develop quantum technologies, quantum effects beyond the Schrödinger equation, as those described by a Dirac equation, are being investigated due to peculiarities of the spectrum, band structure, rich phase diagrams, remarkable transport properties [7,30,31], and control possibilities implied by the coupling between internal states and momentum [32]. This motivates the development of efficient control approaches for Dirac dynamics. The mentioned coupling may be useful for well defined momenta, but also limits the controllability of internal states introducing systematic errors for a wave packet with a non-negligible momentum width. We have demonstrated that inverse engineering based on invariants of motion provides robust protocols for manipulating the qubit in a $1+1$ Dirac system implemented by trapped ions. This example suggests that "shortcuts to adiabaticity" are a useful tool in the broad context of quantum simulations and more generally to develop quantum technologies.

ACKNOWLEDGMENTS

The authors acknowledge support from Spanish MINECO/FEDER Grants No. FIS2015-69983-P and No. FIS2015-67161-P, Basque Government Grant No. IT986-16, Ramón y Cajal Grant No. RYC-2012-11391, UPV/EHU UFI 11/55, the National Natural Science Foundation of China under Grants No. 11474026 and No. 11674033, and the Fundamental Research Funds for the Central Universities under Grant No. 2015KJJCA01.

[1] P. A. M. Dirac, Proc. R. Soc. London, Ser. A **117**, 778 (1928).
[2] B. Thaller, *The Dirac Equation* (Springer, Berlin, 1956).
[3] L. Lamata, J. León, T. Schätz, and E. Solano, Phys. Rev. Lett. **98**, 253005 (2007).
[4] R. Gerritsma, G. Kirchmair, F. Zähringer, E. Solano, R. Blatt, and C. F. Roos, Nature (London) **463**, 68 (2010).
[5] J. Casanova, J. J. García-Ripoll, R. Gerritsma, C. F. Roos, and E. Solano, Phys. Rev. A **82**, 020101(R) (2010).
[6] R. Gerritsma, B. P. Lanyon, G. Kirchmair, F. Zähringer, C. Hempel, J. Casanova, J. J. García-Ripoll, E. Solano, R. Blatt, and C. F. Roos, Phys. Rev. Lett. **106**, 060503 (2011).
[7] T. O. Wehling, A. M. Black-Schaffer, and A. V. Balatsky, Adv. Phys. **63**, 1 (2014).
[8] S. Longhi, Opt. Lett. **35**, 235 (2010).
[9] T. Salger, C. Grossert, S. Kling, and M. Weitz, Phys. Rev. Lett. **107**, 240401 (2011).
[10] D.-W. Zhang, Z.-D. Wang, and S.-L. Zhu, Front. Phys. **7**, 31 (2012).
[11] J. Pedernales, R. Di Candia, D. Ballester, and E. Solano, New J. Phys. **15**, 055008 (2013).
[12] S. Deffner, New J. Phys. **18**, 012001 (2016).
[13] E. Torrontegui, S. Ibáñez, S. Martínez-Garaot, M. Modugno, A. del Campo, D. Guéry-Odelin, A. Ruschhaupt, X. Chen, and J. G. Muga, Adv. At. Mol. Opt. Phys. **62**, 117 (2013).
[14] J. G. Muga, M. A. Simón, and A. Tobalina, New J. Phys. **18**, 021005 (2016).
[15] A. Ruschhaupt, X. Chen, D. Alonso, and J. G. Muga, New J. Phys. **14**, 093040 (2012).
[16] X. J. Lu, X. Chen, A. Ruschhaupt, D. Alonso, S. Guérin, and J. G. Muga, Phys. Rev. A **88**, 033406 (2013).
[17] B. Thaller, *Advanced Visual Quantum Mechanics* (Springer, Berlin, 2004).
[18] S. Masuda and K. Nakamura, Proc. R. Soc. London, Ser. A **466**, 1135 (2010).
[19] S. Masuda and K. Nakamura, Phys. Rev. A **84**, 043434 (2011).
[20] H. R. Lewis and W. B. Riesenfeld, J. Math. Phys. **10**, 1458 (1969).
[21] R. R. Landim and I. Guedes, Phys. Rev. A **61**, 054101 (2000).
[22] A. S. de Castro and A. de Souza Dutra, Phys. Rev. A **67**, 054101 (2003).
[23] B. Khantoul and A. Fring, Phys. Lett. A **379**, 2704 (2015).
[24] Z. G. Zhang, Phys. Scr. **76**, 349 (2007).
[25] J. G. Muga, X. Chen, A. Ruschhaupt, E. Torrontegui, and D. Guéry-Odelin, J. Phys. B **42**, 241001 (2009).
[26] X. Chen, E. Torrontegui, and J. G. Muga, Phys. Rev. A **83**, 062116 (2011).
[27] D. Daems, A. Ruschhaupt, D. Sugny, and S. Guérin, Phys. Rev. Lett. **111**, 050404 (2013).
[28] A. Sørensen and K. Mølmer, Phys. Rev. Lett. **82**, 1971 (1999).
[29] D. Leibfried, R. Blatt, C. Monroe, and D. Wineland, Rev. Mod. Phys. **75**, 281 (2003).
[30] N. Y. Kim, K. Kusudo, A. Löffler, S. Höfling, A. Forchel, and Y. Yamamoto, New J. Phys. **15**, 035032 (2013).
[31] L. Tarruell, D. Greif, T. Uehlinger, G. Jotzu, and T. Esslinger, Nature (London) **483**, 302 (2012).
[32] J. Schliemann, D. Loss, and R. M. Westervelt, Phys. Rev. Lett. **94**, 206801 (2005).